Available online at www.sciencedirect.com
SCIENCE DIRECT®
Wave Motion 43 (2006) 368–386
WAVE MOTION
www.elsevier.com/locate/wavemoti

# Propagation of a mode-III interfacial conductive crack along a conductive interface between two piezoelectric materials

Albert C. To, Shaofan Li *, Steven D. Glaser

*Department of Civil and Environmental Engineering, University of California, Berkeley, CA, USA*

Received 3 April 2005; received in revised form 24 August 2005; accepted 1 February 2006
Available online 19 April 2006

**Abstract**

An analysis is presented for transient response of a mode-III interfacial crack propagating between two dissimilar piezoelectric half spaces. The dynamic fracture toughness of a piezoelectric interface is examined, which is a central issue related to the interface strength of multi-layered sensors and ferroelectric thin film devices.

For the mode-III crack propagation in piezoelectric materials, an electro-acoustic surface wave, the Bleustein–Gulyaev wave, controls the crack propagation speed. It is shown that the propagation of an interfacial crack in piezoelectric media may excite an interfacial electro-acoustic surface wave, the Maerfeld–Tournois wave, which is fundamentally different from the mode-III interfacial crack propagation in purely elastic media. Moreover, it has been discovered that the existence of the Maerfeld–Tournois wave may play a significant role in determining the dynamic fracture toughness for piezoelectric composites.


*Keywords:* Dynamic fracture; Interfacial crack; Maerfeld–Tournois wave; Piezoelectricity

## 1. Introduction

One of the challenging problems in dynamic fracture of piezoelectric media is the problem of interfacial crack propagation in dissimilar piezoelectric media. Much of the current research efforts has focused on static and nonlinear fracture behaviors. Only few of them consider dynamic effects. Among the few contributions to dynamic fracture mechanics of piezoelectric materials, we would like to mention Shindo and Ozawa [31], Dascalu and Maugin [7], Li and Mataga [19,20], Narita and Shindo [22], Li [16,17], and more recently Ing and Wang [14].

Recently, Ru et al. [30,29,27,28] have systematically examined electrode–ceramic interfacial cracks. To the best of the authors' knowledge, the transient behaviors of dynamic electrode–ceramic interfacial crack propagation have never been examined before. Interfacial crack propagation between two dissimilar piezoelectric materials may excite several SH surface waves, e.g., Bleustein–Gulyaev waves in both media, and an interfacial electro-acoustic surface wave – Maerfeld–Tournois (MT) wave [21]. How the presence of these surface waves

* Corresponding author. Tel.: +1 510 642 5362; fax: +1 510 643 8928.
*E-mail address:* li@ce.berkeley.edu (S. Li).

0165-2125/$ - see front matter © 2006 Elsevier B.V. All rights reserved.
doi:10.1016/j.wavemoti.2006.02.001

affect the interfacial crack propagation is an open problem. It is of fundamental importance in establishing a rational physical theory to estimate dynamic fracture toughness of piezoelectric materials.

The presentation of the paper is organized as follows: we first set up the mixed initial boundary problem in Section 2; Section 3 presents the fundamental solution of the dynamic fracture problem in Laplace transform space; in Section 4, the fundamental solution in physical space is derived; and in Section 5, some immediate consequences of the obtained solution are discussed.

## 2. Formulation of the problem

For the mode-III crack propagation problem considered in this paper, the relevant electromechanical couplings are between the anti-plane displacement and the in-plane electric field. They can be expressed as:

$$\mathbf{u} = (0, 0, w(X, Y, t)), \tag{1}$$

$$\mathbf{E} = \left(-\frac{\partial \phi}{\partial X}, -\frac{\partial \phi}{\partial Y}, 0\right). \tag{2}$$

Introduce a pseudo-electric potential function

$$\psi = \phi - \frac{e_{15}}{\epsilon_{11}} C_f w, \tag{3}$$

where $C_f := c_\ell^2/(c_\ell^2 - c_a^2)$, $c_\ell := (\epsilon_{11}\mu_0)^{-1/2}$, $c_a := \sqrt{\bar{c}_{44}/\rho}$, and $\bar{c}_{44} := c_{44}^E + e_{15}^2/\epsilon_{11}$.

Following Li [15], we can derive a system of decoupled wave equations:

$$\left(\frac{\partial^2}{\partial X^2} + \frac{\partial^2}{\partial Y^2} - \frac{1}{c_a^2}\frac{\partial^2}{\partial t^2}\right) w = 0, \tag{4}$$

$$\left(\frac{\partial^2}{\partial X^2} + \frac{\partial^2}{\partial Y^2} - \frac{1}{c_\ell^2}\frac{\partial^2}{\partial t^2}\right) \psi = 0. \tag{5}$$

We employ the so-called "quasi-hyperbolic" approximation, which neglects the rotational electric field but maintains the hyperbolicity of the problem to simplify the governing equations. Readers are referred to [16,32] for further details on the quasi-hyperbolic approximation. Under the quasi-hyperbolic approximation, the relevant constitutive equations are:

$$\sigma_{xz} = \tilde{c}_{44}\frac{\partial w}{\partial X} + e_{15}\frac{\partial \psi}{\partial X}, \tag{6}$$

$$\sigma_{yz} = \tilde{c}_{44}\frac{\partial w}{\partial Y} + e_{15}\frac{\partial \psi}{\partial Y}, \tag{7}$$

$$D_X = e_{15}(1 - C_f)\frac{\partial w}{\partial X} - \epsilon_{11}\frac{\partial \psi}{\partial X}, \tag{8}$$

$$D_Y = e_{15}(1 - C_f)\frac{\partial w}{\partial Y} - \epsilon_{11}\frac{\partial \psi}{\partial Y}, \tag{9}$$

where $\tilde{c}_{44} := \bar{c}_{44}[1 - (1 - C_f)(e_{15}^2/\bar{c}_{44}\epsilon_{11})]$.

### 2.1. Semi-infinite moving crack

Consider a semi-infinite crack located at $Y = 0$, $X < 0$, along an interface between two welded dissimilar piezoelectric half spaces (Fig. 1). It is assumed that the crack is in a state of static equilibrium when $t < 0$, and its leading edge is parallel to the poling direction of the piezoelectric body. At $t = 0^+$, a pair of concentrated longitudinal shear forces are applied on the surfaces of the pre-existing semi-infinite crack, and the crack is assumed to propagate at a constant speed $v$.

In the mode-III crack model considered here, it is expected that several different surface waves can influence the dynamic fracture behavior: the Bleustein–Gulyaev (BG) wave for each of the medium [3,13], the Maerfeld–

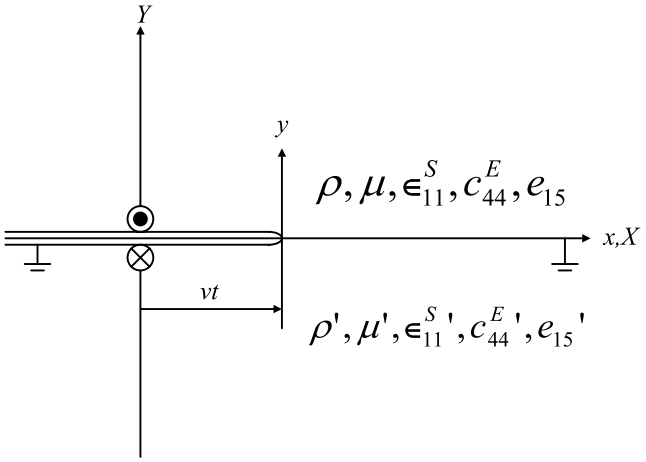


Fig. 1. A running crack subjected to concentrated point load.

Tournois (MT) wave [21], and the shear wave (see also [32]). The complex interaction between all these waves is unseen in any previous dynamic mode-III crack models. The only other dynamic crack model that has such rich behavior is the mode-I semi-infinite interfacial crack in purely elastic materials considered by Brock [4]. In that model, the dynamic fracture behavior is dictated by four different waves: two Rayleigh waves, the Stoneley wave, and the p-wave.

For dynamic fracture problems, it is usually convenient to study the crack propagation in a moving coordinate system $(x, y, z)$, with

$$x = X - vt, \quad y = Y, \quad z = Z. \tag{10}$$

We define the following nondimensional parameters:

$$s_a := (1 - v^2/c_a^2)^{1/2}, \tag{11}$$

$$s_l := (1 - v^2/c_l^2)^{1/2}. \tag{12}$$

By making use of (10), the equations of motion in the moving coordinate system are cast into the form:

$$\begin{aligned} s_a^2 \frac{\partial^2 w}{\partial x^2} + \frac{\partial^2 w}{\partial y^2} + \frac{2v}{c_a^2} \frac{\partial^2 w}{\partial x \partial t} - \frac{1}{c_a^2} \frac{\partial^2 w}{\partial t^2} = 0, \\ s_l^2 \frac{\partial^2 \psi}{\partial x^2} + \frac{\partial^2 \psi}{\partial y^2} + \frac{2v}{c_l^2} \frac{\partial^2 \psi}{\partial x \partial t} - \frac{1}{c_l^2} \frac{\partial^2 \psi}{\partial t^2} = 0. \end{aligned} \tag{13}$$

Without loss of generality, we assume in the rest of the discussion that the acoustic speed in the lower half space $c_a'$ is the slowest among the four wave speeds, $c_a$, $c_a'$, $c_l$, and $c_l'$, where the quantities with prime ($'$) denotes those of the lower piezoelectric half space as shown in Fig. 1.

At infinity, the acoustic displacement and the light wave potential are assumed to vanish:

$$\left.\begin{aligned} w(x, y, t) = 0 \\ \psi(x, y, t) = 0 \end{aligned}\right\} \quad y \to \infty; \tag{14}$$

$$\left.\begin{aligned} w'(x, y, t) = 0 \\ \psi'(x, y, t) = 0 \end{aligned}\right\} \quad y \to -\infty. \tag{15}$$

To find the solution under general loading conditions, we first consider the fundamental solution of transient crack propagation, i.e., crack propagation under a concentrated load acting on the crack surface, so that the following mechanical boundary conditions are imposed:

$$\sigma_{yz}(x, 0, t) = \sigma_{yz}'(x, 0, t) = -\delta(x + vt) H(t), \quad x < 0, \tag{16a}$$

$$w(x,0,t) = w'(x,0,t), \quad x \geqslant 0. \tag{16b}$$

The second equation stems from the continuity condition of the displacement at the interface.

In this paper, we have adopted the conducting crack model, in which the crack surface is assumed to be covered with a thin metal film with infinite conductivity. This is equivalent to assuming that the crack surfaces are coated with an infinitesimally thin, perfectly conducting film that is grounded, i.e.

$$\phi(x,0,t) = \phi'(x,0,t) = 0, \quad -\infty < x < \infty. \tag{17}$$

The full set of boundary conditions considered in this paper can be summarized as:

$$\sigma_{yz}(x,0,t) = \sigma'_{yz}(x,0,t) = -\delta(x+vt)H(t), \quad x < 0, \tag{18}$$

$$w(x,0,t) = w'(x,0,t), \quad x \geqslant 0, \tag{19}$$

$$\phi(x,0,t) = \phi'(x,0,t) = 0, \quad -\infty < x < \infty, \tag{20}$$

with quiescent initial conditions:

$$w(x,y,0) = w'(x,y,0) = 0, \quad \dot{w}(x,y,0) = \dot{w}'(x,y,0) = 0, \tag{21}$$

$$\psi(x,y,0) = \psi'(x,y,0) = 0, \quad \dot{\psi}(x,y,0) = \dot{\psi}'(x,y,0) = 0. \tag{22}$$

## 3. Integral equation solutions

### 3.1. Solution procedures

The standard procedure of multiple Laplace transforms is employed to seek the solution of the above mixed initial boundary value problem. The multiple transforms are introduced for the variable pair $(x,t)$. To suppress the time variable $t$, the usual, one-sided Laplace transform is applied:

$$f^*(x,y,p) = \int_0^\infty f(x,y,t)\,\exp(-pt)\,\mathrm{d}t, \tag{23}$$

$$f(x,y,t) = \frac{1}{2\pi \mathrm{i}} \int_{Br_1} f^*(x,y,p)\exp(pt)\,\mathrm{d}p, \tag{24}$$

where the inversion integration is taken over the usual Bromwich path.

To suppress the spatial variable $x$, the two-sided Laplace transform is used:

$$\hat{f}^*(\zeta,y,p) = \int_{-\infty}^\infty f^*(x,y,p)\,\exp(-p\zeta x)\,\mathrm{d}x, \tag{25}$$

$$f^*(x,y,p) = \frac{p}{2\pi \mathrm{i}} \int_{Br_2} \hat{f}^*(\zeta,y,p)\,\exp(p\zeta x)\,\mathrm{d}\zeta. \tag{26}$$

After transformation, the governing equations (4) and (5) become:

$$\left.\begin{aligned} &\left[\frac{\mathrm{d}^2}{\mathrm{d}y^2} - p^2\left(\frac{1}{c_a^2} - 2\frac{v}{c_a^2}\zeta - s_a^2\zeta^2\right)\right]\hat{w}^*(\zeta,y,p) = 0 \\ &\left[\frac{\mathrm{d}^2}{\mathrm{d}y^2} - p^2\left(\frac{1}{c_l^2} - 2\frac{v}{c_l^2}\zeta - s_l^2\zeta^2\right)\right]\hat{\psi}^*(\zeta,y,p) = 0 \end{aligned}\right\} y > 0, \tag{27}$$

$$\left.\begin{aligned} &\left[\frac{\mathrm{d}^2}{\mathrm{d}y^2} - p^2\left(\frac{1}{c_a'^2} - 2\frac{v}{c_a'^2}\zeta - s_a'^2\zeta^2\right)\right]\hat{w}'^*(\zeta,y,p) = 0 \\ &\left[\frac{\mathrm{d}^2}{\mathrm{d}y^2} - p^2\left(\frac{1}{c_l'^2} - 2\frac{v}{c_l'^2}\zeta - s_l'^2\zeta^2\right)\right]\hat{\psi}'^*(\zeta,y,p) = 0 \end{aligned}\right\} y < 0. \tag{28}$$

To satisfy the boundary conditions at infinity, we choose the solution of the following form:

$$\left.\begin{aligned}\hat{w}^*(\zeta,y,p) &= \tfrac{1}{p^2}A(\zeta)\exp(-p\alpha y)\\ \hat{\psi}^*(\zeta,y,p) &= \tfrac{1}{p^2}B(\zeta)\exp(-p\beta y)\end{aligned}\right\} y>0, \tag{29}$$

$$\left.\begin{aligned}\hat{w}'^*(\zeta,y,p) &= -\tfrac{1}{p^2}A'(\zeta)\exp(p\alpha' y)\\ \hat{\psi}'^*(\zeta,y,p) &= -\tfrac{1}{p^2}B'(\zeta)\exp(p\beta' y)\end{aligned}\right\} y<0. \tag{30}$$

The coefficient functions $\alpha$, $\beta$, $\alpha'$, and $\beta'$ are written as:

$$\alpha(\zeta) := \sqrt{\frac{1}{c_a^2}-\frac{2v\zeta}{c_a^2}-s_a^2\zeta^2} = s_a\sqrt{\left(\zeta+\frac{1}{c_a-v}\right)\left(\frac{1}{c_a+v}-\zeta\right)}, \tag{31}$$

$$\beta(\zeta) := \sqrt{\frac{1}{c_l^2}-\frac{2v\zeta}{c_l^2}-s_l^2\zeta^2} = s_l\sqrt{\left(\zeta+\frac{1}{c_l-v}\right)\left(\frac{1}{c_l+v}-\zeta\right)}, \tag{32}$$

$$\alpha'(\zeta) := \sqrt{\frac{1}{c_a'^2}-\frac{2v\zeta}{c_a'^2}-s_a'^2\zeta^2} = s_a'\sqrt{\left(\zeta+\frac{1}{c_a'-v}\right)\left(\frac{1}{c_a'+v}-\zeta\right)}, \tag{33}$$

$$\beta'(\zeta) := \sqrt{\frac{1}{c_l'^2}-\frac{2v\zeta}{c_l'^2}-s_l'^2\zeta^2} = s_l'\sqrt{\left(\zeta+\frac{1}{c_l'-v}\right)\left(\frac{1}{c_l'+v}-\zeta\right)}. \tag{34}$$

Substituting the solutions (29), (30) into the transformed electrical boundary condition Eq. (20), one finds that

$$B(\zeta) = -\frac{e_{15}}{\epsilon_{11}}C_f A(\zeta) \quad \text{and} \quad B'(\zeta) = -\frac{e'_{15}}{\epsilon'_{11}}C'_f A'(\zeta). \tag{35}$$

Now, the displacement and the light wave potential in $y>0$ can be expressed in terms of a single unknown function $A(\zeta)$:

$$w^*(x,y,p) = \frac{1}{2\pi i p}\int_{\zeta_\alpha-i\infty}^{\zeta_\alpha+i\infty} A(\zeta)\exp[-p(\alpha y-\zeta x)]\,d\zeta, \tag{36}$$

$$\psi^*(x,y,p) = -\frac{e_{15}C_f}{2\pi i p\epsilon_{11}}\int_{\zeta_\beta-i\infty}^{\zeta_\beta+i\infty} A(\zeta)\exp[-p(\beta y-\zeta x)]\,d\zeta. \tag{37}$$

### 3.2. The Wiener–Hopf decomposition

We use the Wiener–Hopf decomposition technique to find the solution in transformed space. To apply the Wiener–Hopf technique, it is expedient to expand the mechanical boundary conditions over the full range of the $x$-axis. This can be done by introducing two unknown functions:

$$\sigma_+(x,t) := \begin{cases}\sigma_{yz}(x,0,t)=\sigma'_{yz}(x,0,t), & x\geqslant 0,\\ 0, & x<0,\end{cases} \tag{38}$$

$$\Delta w_-(x,t) := \begin{cases}0, & x\geqslant 0,\\ w(x,0,t)-w'(x,0,t), & x<0,\end{cases} \tag{39}$$

such that:

$$\sigma_{yz}(x,0,t)=\sigma'_{yz}(x,0,t)=\sigma_+(x,t)-\delta(x+vt)H(t), \quad -\infty<x<\infty, \tag{40}$$

$$w(x,0,t)-w'(x,0,t)=\Delta w_-(x,t)+0, \quad -\infty<x<\infty. \tag{41}$$

After suppressing both $x$ and $t$:

$$\hat{\sigma}^*_{yz}(\zeta,0,p) = \hat{\sigma}'^*_{yz}(\zeta,0,p) = \frac{\Sigma_+(\zeta)}{p} + \frac{1}{pv}\frac{1}{(\zeta - 1/v)}, \tag{42}$$

$$\hat{w}^*(\zeta,0,p) - \hat{w}'^*(\zeta,0,p) = \frac{\Delta U_-(\zeta)}{p^2}, \tag{43}$$

where:

$$\Sigma_+(\zeta) := p\int_0^\infty \sigma^*_+(x,p)\,\exp(-p\zeta x)\,\mathrm{d}x, \tag{44}$$

$$\Delta U_-(\zeta) := p^2\int_{-\infty}^0 \Delta w^*_-(x,p)\exp(-p\zeta x)\,\mathrm{d}x. \tag{45}$$

On the other hand, substituting (29), (30), and (35) into the transformed constitutive equations for the stresses $\sigma_{yz}$ and $\sigma'_{yz}$, one obtains

$$A(\zeta) = -\frac{p}{D(\zeta)}\hat{\sigma}^*_{yz}(\zeta,0,p) \text{ and } A'(\zeta) = -\frac{p}{D'(\zeta)}\hat{\sigma}'^*_{yz}(\zeta,0,p), \tag{46}$$

where

$$D(\zeta) = \tilde{c}_{44}(\alpha(\zeta) - \tilde{k}_e^2\beta(\zeta)) \text{ and } D'(\zeta) = \tilde{c}'_{44}(\alpha'(\zeta) - \tilde{k}'^2_e\beta'(\zeta)), \tag{47}$$

are recognized as the Bleustein–Gulyaev wave functions [3,13] modified by the prescribed velocity $v$ for the upper and lower piezoelectric half spaces, respectively. $\tilde{k}_e^2$ and $\tilde{k}'^2_e$ are the electro-mechanical coupling coefficients

$$\tilde{k}_e^2 := \frac{e_{15}^2}{\epsilon_{11}\tilde{c}_{44}}C_f \text{ and } \tilde{k}'^2_e := \frac{{e'_{15}}^2}{\epsilon'_{11}\tilde{c}'_{44}}C'_f. \tag{48}$$

Substituting (29), (30), and (46) into the displacement boundary condition (43) leads to the standard Wiener–Hopf equation

$$\Sigma_+(\zeta) + \frac{1}{v(\zeta - 1/v)} = K(\zeta)\Delta U_-(\zeta) \tag{49}$$

with

$$K(\zeta) := -\frac{D(\zeta)D'(\zeta)}{M(\zeta)}, \tag{50}$$

where

$$M(\zeta) := D(\zeta) + D'(\zeta), \tag{51}$$

is recognized as the Maerfeld–Tournois wave function modified by the prescribed propagating velocity $v$ [21].

The key to solving the Wiener–Hopf equation (49) is to factorize $K(\zeta)$ into sectionally analytic functions in the left and right half complex-$\zeta$ planes, respectively.

Define the Bleustein–Gulyaev wave speeds for upper and lower half spaces, respectively

$$c_{\mathrm{bg}} := c_a\sqrt{\tilde{C}_f(1-\tilde{k}_e^4)} \text{ and } c'_{\mathrm{bg}} := c'_a\sqrt{\tilde{C}'_f(1-\tilde{k}'^4_e)}, \tag{52}$$

where

$$\tilde{C}_f := \frac{c_l^2}{c_l^2 - \tilde{k}_e^4 c_a^2} \text{ and } \tilde{C}'_f := \frac{c_l'^2}{c_l'^2 - \tilde{k}_e'^4 c_a'^2}. \tag{53}$$

The product decomposition of Bleustein–Gulyaev function is given by Li and Mataga [19] or in [16]:

$$D(\zeta) = \frac{(1/(c_{\mathrm{bg}} - v) + \zeta)(1/(c_{\mathrm{bg}} + v) - \zeta)}{\sqrt{(1/(c_a - v) + \zeta)(1/(c_a + v) - \zeta)}}\mathcal{T}_+(\zeta)\mathcal{T}_-(\zeta)D_s(v), \tag{54}$$

$$D'(\zeta) = \frac{(1/(c'_{\mathrm{bg}} - v) + \zeta)(1/(c'_{\mathrm{bg}} + v) - \zeta)}{\sqrt{(1/(c'_a - v) + \zeta)(1/(c'_a + v) - \zeta)}} \mathcal{T}'_+(\zeta)\mathcal{T}'_-(\zeta) D'_s(v), \tag{55}$$

where

$$D_s(v) := \tilde{c}_{44}(s_a - \tilde{k}_e^2 s_l) \text{ and } D'_s(v) := \tilde{c}'_{44}(s'_a - \tilde{k}_e'^2 s'_l) \tag{56}$$

and

$$\begin{aligned} \mathcal{T}_\pm(\zeta) &:= \exp\left\{ -\frac{1}{\pi} \int_{1/(c_l \mp v)}^{1/(c_a \mp v)} \arctan\left[\frac{\Im(D(\mp\eta))}{\Re(D(\mp\eta))}\right] \frac{\mathrm{d}\eta}{\eta \pm \zeta} \right\}, \\ \mathcal{T}'_\pm(\zeta) &:= \exp\left\{ -\frac{1}{\pi} \int_{1/(c'_l \mp v)}^{1/(c'_a \mp v)} \arctan\left[\frac{\Im(D'(\mp\eta))}{\Re(D'(\mp\eta))}\right] \frac{\mathrm{d}\eta}{\eta \pm \zeta} \right\}. \end{aligned} \tag{57}$$

The Maerfeld–Tournois wave exists if there exists a real root $v$ to the following Maerfeld–Tournois wave equation:

$$D_s(v) + D'_s(v) = 0, \tag{58}$$

where $D_s(v)$ and $D'_s(v)$ are Bleustein–Gulyaev wave functions defined in (56). The real root $v = c_{\mathrm{mt}}$ that satisfies (58) is called the Maerfeld–Tournois (MT) wave speed.

Define $c$ as follows:

$$c := \begin{cases} c_{\mathrm{mt}} & \text{if the Maerfeldwave exists,} \\ c'_a, & \text{otherwise.} \end{cases} \tag{59}$$

It can be shown that the Maerfeld–Tournois wave function, $M(\zeta)$, can be factorized as products of sectionally analytic functions

$$M(\zeta) = \frac{(1/(c - v) + \zeta)(1/(c + v) - \zeta)}{\sqrt{(1/(c'_a - v) + \zeta)(1/(c'_a + v) - \zeta)}} \mathcal{S}_+(\zeta)\mathcal{S}_-(\zeta) \cdot (D_s(v) + D'_s(v)), \tag{60}$$

where

$$\mathcal{S}_\pm(\zeta) := \exp\left\{ -\frac{1}{\pi} \int_{1/(c_{\max} \mp v)}^{1/(c_{\min} \mp v)} \arctan\left[\frac{\Im(M(\mp\eta))}{\Re(M(\mp\eta))}\right] \frac{\mathrm{d}\eta}{\eta \pm \zeta} \right\}, \tag{61}$$

where $c_{\max}$ and $c_{\min}$ are, respectively, the maximum and minimum of the four wave speeds, $c_a$, $c'_a$, $c_l$, and $c'_l$. The product factorization of $M(\zeta)$ is quite different from those of $D(\zeta)$ and $D'(\zeta)$, because it depends on the existence of the Maerfeld–Tournois wave.

We now can solve the Wiener–Hopf equation (49). First, define

$$Q(v) := \frac{D_s(v)D'_s(v)}{D_s(v) + D'_s(v)}, \; F_+(\zeta) := \frac{\mathcal{T}_+(\zeta)\mathcal{T}'_+(\zeta)}{\mathcal{S}_+(\zeta)}, \text{ and } F_-(\zeta) := \frac{\mathcal{T}_-(\zeta)\mathcal{T}'_-(\zeta)}{\mathcal{S}_-(\zeta)} \tag{62}$$

and

$$G_+(\zeta) := \frac{1}{F_+(\zeta)} \frac{(1/(c - v) + \zeta)\sqrt{(1/(c_a - v) + \zeta)}}{(1/(c_{\mathrm{bg}} - v) + \zeta)(1/(c'_{\mathrm{bg}} - v) + \zeta)}. \tag{63}$$

Following the procedure in Noble [23], the solution to the Wiener–Hopf equation (49) is:

$$\Sigma_+(\zeta) = \frac{1}{v(\zeta - 1/v)} \left( \frac{G_+(1/v)}{G_+(\zeta)} - 1 \right), \tag{64}$$

$$\Delta U_-(\zeta) = -\frac{(1/(c + v) - \zeta)\sqrt{(1/(c_a + v) - \zeta)}}{v(\zeta - 1/v)(1/(c_{\mathrm{bg}} + v) - \zeta)(1/(c'_{\mathrm{bg}} + v) - \zeta)} \cdot \frac{G_+(1/v)}{Q(v)F_-(\zeta)}. \tag{65}$$

The functions $A(\zeta)$ and $A'(\zeta)$ are then obtained by substituting Eqs. (64), (65), and (43) into Eq. (46):

$$A(\zeta) = -\frac{G_+(\zeta)}{\tilde{c}_{44}(\alpha(\zeta) - \tilde{k}_e^2\beta(\zeta))v(\zeta - 1/v)G_+(\zeta)}$$
$$= -\frac{(c_{\mathrm{bg}} - v)(c'_{\mathrm{bg}} - v)}{\tilde{c}_{44}(\alpha(\zeta) - \tilde{k}_e^2\beta(\zeta))v(\zeta - 1/v)c_{\mathrm{bg}}c'_{\mathrm{bg}}(c - v)} \cdot \sqrt{\frac{vc_a}{c_a - v}} \frac{(1/(c_{\mathrm{bg}} - v) + \zeta)(1/(c'_{\mathrm{bg}} - v) + \zeta)}{(1/(c - v) + \zeta)\sqrt{(1/(c_a - v) + \zeta)}}$$
$$\times \frac{F_+(\zeta)}{F_+(1/v)}, \tag{66}$$

$$A'(\zeta) = -\frac{G_+(1/v)}{\tilde{c}'_{44}(\alpha'(\zeta) - \tilde{k}'^2_e\beta'(\zeta))v(\zeta - 1/v)G_+(\zeta)}$$
$$= -\frac{c(c_{\mathrm{bg}} - v)(c'_{\mathrm{bg}} - v)}{\tilde{c}'_{44}(\alpha'(\zeta) - \tilde{k}'^2_e\beta'(\zeta))v(\zeta - 1/v)c_{\mathrm{bg}}c'_{\mathrm{bg}}(c - v)} \cdot \sqrt{\frac{vc_a}{c_a - v}} \frac{(1/(c_{\mathrm{bg}} - v) + \zeta)(1/(c'_{\mathrm{bg}} - v) + \zeta)}{(1/(c - v) + \zeta)\sqrt{(1/(c_a - v) + \zeta)}}$$
$$\times \frac{F_+(\zeta)}{F_+(1/v)}. \tag{67}$$

The functions $B(\zeta)$ and $B'(\zeta)$ are then obtained by Eq. (35).

## 4. Solutions in the physical domain

Having carried out the Wiener–Hopf decomposition, we are now in a position to invert the integrals in Eqs. (36) and (37) to obtain the explicit solution in the physical domain. This inversion can be done by using the Cagniard-de Hoop scheme [5,8].

### 4.1. The Cagniard–de Hoop procedure

We proceed by replacing the original Bromwich path by a deformed Cagniard contour such that the one-sided Laplace transform can be obtained by inspection. We seek particular contours in the $\zeta$-plane (see Fig. 2) along which the exponentials in each integral of Eqs. (36) and (37) take the form $\exp(-pt)$. To achieve this, we let

$$\alpha(\zeta)y - \zeta x = t. \tag{68}$$

Then the first set of deformed paths are obtained as

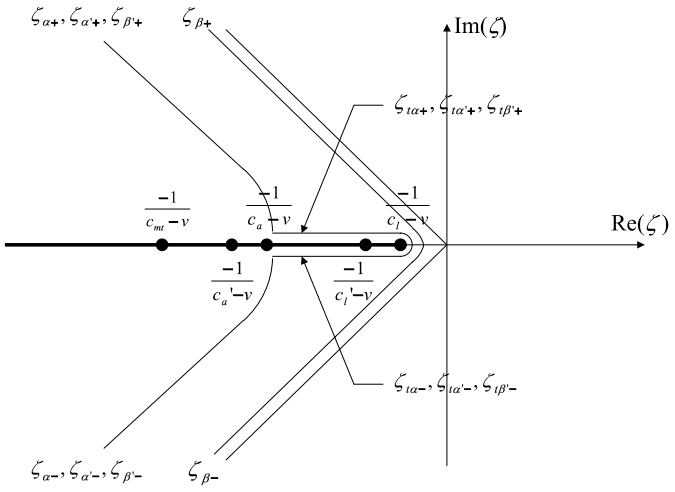


Fig. 2. Cagniard–de Hoop contours in $\zeta$-plane.

$$\zeta_{\alpha\pm} = \frac{1}{x^2 + s_a^2 y^2}\left(-\left(tx + \frac{v}{c_a^2}y^2\right) \pm \mathrm{i}y\sqrt{s_a^2 t^2 - \frac{2v}{c_a^2}xt - \frac{r^2}{c_a^2}}\right), \tag{69}$$

where $r^2 = x^2 + y^2$.

The inversion path $\zeta_{\alpha\pm}$ intercepts the $\mathrm{Re}(\zeta)$ axis at the location

$$\zeta_{\alpha i} = -\frac{1}{s_a^2\, c_a}\left[\frac{v}{c_a} + \frac{x}{\sqrt{x^2 + s_a^2 y^2}}\right] \text{ at } t_\alpha = \frac{1}{s_a^2}\left[\frac{vx}{c_a^2} + \frac{1}{c_a}\sqrt{x^2 + s_a^2 y^2}\right]. \tag{70}$$

It can be verified that

$$\frac{-1}{c_a - v} < \zeta_{\alpha i} < \frac{1}{c_a + v}. \tag{71}$$

As shown in Fig. 2, the contour $\zeta_{\alpha\pm}$ may intercept the $\mathrm{Re}(\zeta)$ axis through the branch cut. Therefore, for $\zeta_{\alpha\pm}$, a supplemental contour $\zeta_{t\alpha}$ may be needed consisting of two straight segments and a circle of radius $\delta(\delta \to 0)$ centered at the end of the branch cut at $\zeta = -1/(c_l - v)$. The two segments are represented by

$$\zeta_{t\alpha\pm} = \frac{1}{x^2 + s_a^2 y^2}\left(-\left(xt + \frac{v}{c_a^2}y^2\right) + y\sqrt{\frac{2vxt}{c_a^2} + \frac{r^2}{c_a^2} - s_a^2 t^2}\right) \pm \mathrm{i}\delta. \tag{72}$$

for the following range of $t$:

$$t_{\alpha 0} \leqslant t \leqslant t_\alpha, \tag{73}$$

where:

$$t_{\alpha 0} = \frac{x}{c_l - v} + \frac{y}{c_a(c_l - v)}\sqrt{c_l^2 - c_a^2} \tag{74}$$

for

$$\zeta(t_{\alpha 0}) = -\frac{1}{c_l - v}. \tag{75}$$

Similarly, for the second set of deformed paths, let

$$\beta(\zeta)y - \zeta x = t. \tag{76}$$

Then the second set of deformed paths is obtained as

$$\zeta_{\beta\pm} = \frac{1}{x^2 + s_l^2 y^2}\left(-\left(tx + \frac{v}{c_l^2}y^2\right) \pm \mathrm{i}y\sqrt{s_l^2 t^2 - \frac{2v}{c_l^2}xt - \frac{r^2}{c_l^2}}\right). \tag{77}$$

The inversion path $\zeta_{\beta\pm}$ intercepts the $\mathrm{Re}(\zeta)$ axis at the location

$$\zeta_{\beta i} = -\frac{1}{s_l^2\, c_l}\left[\frac{v}{c_l} + \frac{x}{\sqrt{x^2 + s_l^2 y^2}}\right] \text{ at } t_\beta = \frac{1}{s_l^2}\left[\frac{vx}{c_l^2} + \frac{1}{c_l}\sqrt{x^2 + s_l^2 y^2}\right], \tag{78}$$

where

$$\frac{-1}{c_l - v} < \zeta_{\beta i} < \frac{1}{c_l + v}. \tag{79}$$

As shown in Fig. 2, the contour $\zeta_{\beta\pm}$ always avoids the branch cut, and so there is no need to deform the integration path as in the case for $\zeta_{\alpha\pm}$.

For the third and forth set of integration paths, let

$$-\alpha'(\zeta)y - \zeta x = t \tag{80}$$

and

$$-\beta'(\zeta)y-\zeta x=t, \tag{81}$$

respectively. The procedure is identical to the first and second sets of integration paths and will not be presented here.

As a result of the foregoing manipulations, the closed form solutions can be found directly from the inversion integrals along the Cagniard contours for $y>0$:

$$w(x,y,t)=\frac{1}{\pi}\int_{t_\alpha}^{t}\mathrm{Im}\left[A(\zeta_{\alpha+}(\tau))\frac{\partial\zeta_{\alpha+}(\tau)}{\partial\tau}\right]\mathrm{d}\tau, \tag{82}$$

$$\psi(x,y,t)=-\frac{1}{\pi}\frac{e_{15}}{\epsilon_{11}}C_f'\int_{t_\beta}^{t}\mathrm{Im}\left[A(\zeta_{\beta+}(\tau))\frac{\partial\zeta_{\beta+}(\tau)}{\partial\tau}\right]\mathrm{d}\tau, \tag{83}$$

$$\sigma_{xz}(x,y,t)=\frac{\tilde{c}_{44}}{\pi}\left(H(t-t_\alpha)\mathrm{Im}\left[\zeta_{\alpha+}A(\zeta_{\alpha+})\frac{\partial\zeta_{\alpha+}}{\partial t}\right]-\tilde{k}_e^2H(t-t_\beta)\mathrm{Im}\left[\zeta_{\beta+}A(\zeta_{\beta+})\frac{\partial\zeta_{\beta+}}{\partial t}\right]\right), \tag{84}$$

$$\sigma_{yz}(x,y,t)=-\frac{\tilde{c}_{44}}{\pi}\left(H(t-t_\alpha)\mathrm{Im}\left[\alpha(\zeta_{\alpha+})A(\zeta_{\alpha+})\frac{\partial\zeta_{\alpha+}}{\partial t}\right]-\tilde{k}_e^2H(t-t_\beta)\mathrm{Im}\left[\beta(\zeta_{\beta+})A(\zeta_{\beta+})\frac{\partial\zeta_{\beta+}}{\partial t}\right]\right), \tag{85}$$

$$D_x(x,y,t)=\frac{e_{15}(1-C_f)}{\pi}H(t-t_\alpha)\mathrm{Im}\left[\zeta_{\alpha+}A(\zeta_{\alpha+})\frac{\partial\zeta_{\alpha+}}{\partial t}\right]-\frac{e_{15}}{\pi}H(t-t_\beta)\mathrm{Im}\left[\zeta_{\beta+}A(\zeta_{\beta+})\frac{\partial\zeta_{\beta+}}{\partial t}\right], \tag{86}$$

$$D_y(x,y,t)=-\frac{e_{15}(1-C_f)}{\pi}H(t-t_\alpha)\mathrm{Im}\left[\alpha(\zeta_{\alpha+})A(\zeta_{\alpha+})\frac{\partial\zeta_{\alpha+}}{\partial t}\right]+\frac{e_{15}}{\pi}H(t-t_\beta)\mathrm{Im}\left[\beta(\zeta_{\beta+})A(\zeta_{\beta+})\frac{\partial\zeta_{\beta+}}{\partial t}\right]. \tag{87}$$

Similarly, for $y<0$, the closed form solutions are obtained:

$$w'(x,y,t)=-\frac{1}{\pi}\int_{t_{\alpha'}}^{t}\mathrm{Im}\left[A'(\zeta_{\alpha'+}(\tau))\frac{\partial\zeta_{\alpha'+}(\tau)}{\partial\tau}\right]\mathrm{d}\tau, \tag{88}$$

$$\psi'(x,y,t)=-\frac{1}{\pi}\frac{e'_{15}}{\epsilon'_{11}}C_f'\int_{t_{\beta'}}^{t}\mathrm{Im}\left[A'(\zeta_{\beta'+}(\tau))\frac{\partial\zeta_{\beta'+}(\tau)}{\partial\tau}\right]\mathrm{d}\tau, \tag{89}$$

$$\sigma'_{xz}(x,y,t)=-\frac{\tilde{c}'_{44}}{\pi}\left(H(t-t_{\alpha'})\mathrm{Im}\left[\zeta_{\alpha'+}A'(\zeta_{\alpha'+})\frac{\partial\zeta_{\alpha'+}}{\partial t}\right]-\tilde{k}_e'^2H(t-t_{\beta'})\mathrm{Im}\left[\zeta_{\beta'+}A'(\zeta_{\beta'+})\frac{\partial\zeta_{\beta'+}}{\partial t}\right]\right), \tag{90}$$

$$\sigma'_{yz}(x,y,t)=-\frac{\tilde{c}'_{44}}{\pi}\left(H(t-t_{\alpha'})\mathrm{Im}\left[\alpha'(\zeta_{\alpha'+})A'(\zeta_{\alpha'+})\frac{\partial\zeta_{\alpha'+}}{\partial t}\right]-\tilde{k}_e'^2H(t-t_{\beta'})\mathrm{Im}\left[\beta'(\zeta_{\beta'+})A'(\zeta_{\beta'+})\frac{\partial\zeta_{\beta'+}}{\partial t}\right]\right), \tag{91}$$

$$D'_x(x,y,t)=-\frac{e'_{15}(1-C'_f)}{\pi}H(t-t_{\alpha'})\mathrm{Im}\left[\zeta_{\alpha'+}A'(\zeta_{\alpha'+})\frac{\partial\zeta_{\alpha'+}}{\partial t}\right]+\frac{e'_{15}}{\pi}H(t-t_{\beta'})\mathrm{Im}\left[\zeta_{\beta'+}A'(\zeta_{\beta'+})\frac{\partial\zeta_{\beta'+}}{\partial t}\right], \tag{92}$$

$$\begin{aligned}D'_y(x,y,t)=&-\frac{e'_{15}(1-C'_f)}{\pi}H(t-t_{\alpha'})\mathrm{Im}\left[\alpha'(\zeta_{\alpha'+})A'(\zeta_{\alpha'+})\frac{\partial\zeta_{\alpha'+}}{\partial t}\right]\\&+\frac{e'_{15}}{\pi}H(t-t_{\beta'})\mathrm{Im}\left[\beta'(\zeta_{\beta'+})A'(\zeta_{\beta'+})\frac{\partial\zeta_{\beta'+}}{\partial t}\right].\end{aligned} \tag{93}$$

It may be verified that if materials in the upper and lower half spaces are identical, the above solutions recover the solution for anti-plane crack propagation obtained by Li and Mataga [19].

### 4.2. Intensity factors

Before deriving dynamic intensity factors, we first use superposition to find the solution corresponding to the distributed loading case. Assume a general antisymmetric external load distribution, $p(X)$, over the newly formed crack surface ($0<X<vt$). The general stress field and electric displacement field ahead of the crack tip are then obtained from the fundamental solutions as:

$$\sigma^{(g)}(x,t) = \int_0^{vt} \sigma_{yz}\left(x,0,t-\frac{X}{v}\right)p(X)\,\mathrm{d}X, \tag{94}$$

$$D_y^{(g)}(x,t) = \int_0^{vt} D_y\left(x,0,t-\frac{X}{v}\right)p(X)\,\mathrm{d}X, \tag{95}$$

$$D_y'^{(g)}(x,t) = \int_0^{vt} D_y'\left(x,0,t-\frac{X}{v}\right)p(X)\,\mathrm{d}X, \tag{96}$$

Making the change of variable $vt - X = \eta$ and introducing

$$P(l) := \sqrt{\frac{2}{\pi}}\int_0^l \eta^{-1/2}p(l-\eta)\,\mathrm{d}\eta, \tag{97}$$

the dynamic stress intensity factor for this general load distribution is

$$K_{IIIT}^{(\sigma)}(vt,v) := \lim_{x\to 0}\sqrt{2\pi x}\sigma^{(g)}(x,t) = -\frac{(1-v/c_{\mathrm{bg}})(1-v/c'_{\mathrm{bg}})}{(1-v/c)\sqrt{(1-v/c_a)}}\frac{P(vt)}{F_+(1/v)} \tag{98}$$

and the electric displacement intensity factors are

$$K_{IIIT}^{(D)}(vt,v) := \lim_{x\to 0}\sqrt{2\pi x}D_y^{(g)}(x,t) = \frac{e_{15}((1-C_f)s_a - s_l)}{\tilde{c}_{44}(s_a - \tilde{k}_e^2 s_l)}\cdot\frac{(1-v/c_{\mathrm{bg}})(1-v/c'_{\mathrm{bg}})}{(1-v/c)\sqrt{1-v/c_a}}\frac{P(vt)}{F_+(1/v)} \tag{99}$$

and

$$K_{IIIT}^{(D')}(vt,v) := \lim_{x\to 0}\sqrt{2\pi x}D_y'^{(g)}(x,t) = \frac{e'_{15}((1-C'_f)s'_a - s'_l)}{\tilde{c}'_{44}(s'_a - \tilde{k}'^2_e s'_l)}\cdot\frac{(1-v/c_{\mathrm{bg}})(1-v/c'_{\mathrm{bg}})}{(1-v/c)\sqrt{1-v/c_a}}\frac{P(vt)}{F_+(1/v)}, \tag{100}$$

where the following denotation of the intensity factors is adopted: the superscripts $(\sigma)$, $(D)$, and $(D')$ indicate stress and electric displacements for the respective upper and lower piezoelectric half spaces; the subscript $(IIIT)$ indicates that the loading is an antiplane traction loading.

Following Freund [10], it is convenient to introduce a normalization based on the corresponding "quasi-static" intensity factors. The relevant intensity factors are:

$$K_{IIIT}^{(\sigma)}(vt,0) = -P(vt), \tag{101}$$

$$K_{IIIT}^{(D)}(vt,0) = -\frac{e_{15}}{\tilde{c}_{44}}\frac{C_f}{1-\tilde{k}_e^2}P(vt), \tag{102}$$

and

$$K_{IIIT}^{(D')}(vt,0) = -\frac{e'_{15}}{\tilde{c}'_{44}}\frac{C'_f}{1-\tilde{k}'^2_e}P(vt). \tag{103}$$

Hence, the dynamic intensity factors can be expressed as:

$$K_{IIIT}^{(\sigma)}(vt,v) = f(v)K_{IIIT}^{(\sigma)}(vt,0), \tag{104}$$

$$K_{IIIT}^{(D)}(vt,v) = g(v)K_{IIIT}^{(D)}(vt,0), \tag{105}$$

$$K_{IIIT}^{(D')}(vt,v) = g'(v)K_{IIIT}^{(D')}(vt,0), \tag{106}$$

where:

$$f(v) := \frac{(1-v/c_{\mathrm{bg}})(1-v/c'_{\mathrm{bg}})}{(1-v/c)\sqrt{1-v/c_a}}\frac{1}{F_+(1/v)}, \tag{107}$$

$$g(v) := (1-\tilde{k}_e^2)\frac{(C_f-1)s_a + s_l}{C_f(s_a - \tilde{k}_e^2 s_l)}f(v), \tag{108}$$

$$g'(v) := (1-\tilde{k}_e'^2)\frac{(C_f'-1)s_a'+s_l'}{C_f'(s_a'-\tilde{k}_e'^2 s_l')}f(v), \tag{109}$$

are the nondimensional dynamic intensity factor.

As is the case for the normalized stress intensity factor in the elastodynamic case (to which $f(v)$ reduces when $\tilde{k}_e, \tilde{k}_e' \to 0$), $f(v)$, $g(v)$ and $g'(v)$ are independent of the load distribution function $p(X)$ and the crack extension distance $vt$. They only depend on crack speed and the material constants, which include the Maerfeld–Tournois wave speed or the shear wave speed $c$, the Bleustein–Gulyaev wave speed $c_{\mathrm{bg}}$ and $c_{\mathrm{bg}}'$ in the upper and lower piezoelectric media, and the electro-mechanical coupling factors $\tilde{k}_e$ and $\tilde{k}_e'$. That is, $f$, $g$, and $g'$ are universal functions of piezoelectric dynamic crack growth.

### 4.3. Dynamic free-energy release rate

It has been well established that the free-energy or electric free-enthalpy release rate is the main criterion for fracture toughness in piezoelectric materials, e.g. [24,12,18]. The free-energy release rate criterion has been extensively and exclusively used as the laboratory measurement in experiments, i.e. [26,25,33].

The dynamic energy release rate has also been a standard criterion as well as the standard measurement for the dynamic fracture toughness of a purely elastic medium (see [11]). In piezoelectric media, its counterpart, the dynamic free-enthalpy release rate, has been proposed as the measurement for the dynamic fracture toughness by several authors, e.g. [6,19].

For the interfacial crack studied in this paper, the dynamic free-energy release rate can be calculated as follows:

$$\begin{aligned} G(vt,v) := &\lim_{l\to 0}\int_{-l}^{l}\left[\sigma_{yz}(x,0,t)\frac{\partial w}{\partial x}(x,0,t)+D_y(x,0,t)\frac{\partial \phi}{\partial x}(x,0,t)+vE\right]\mathrm{d}x \\ &-\lim_{l\to 0}\int_{l}^{-l}\left[\sigma_{yz}'(x,0,t)\frac{\partial w'}{\partial x}(x,0,t)+D_y'(x,0,t)\frac{\partial \phi'}{\partial x}(x,0,t)+vE'\right]\mathrm{d}x. \end{aligned} \tag{110}$$

For a conducting crack, the electrostatic potential is zero both along the line ahead of the crack and on the crack faces; consequently, there is no contribution from electric field to the dynamic free energy release rate, and therefore, the free-energy release rate is the same as the purely mechanical energy release rate

$$G(vt,v) := \lim_{l\to 0}\int_{-l}^{l}\left[\sigma_{yz}(x,0,t)\frac{\partial w}{\partial x}(x,0,t)+\sigma_{yz}'(x,0,t)\frac{\partial w'}{\partial x}(x,0,t)\right]\mathrm{d}x, \tag{111}$$

which can be measured in an experiment.

Making use of the identity

$$\lim_{\ell\to 0}\int_{-\ell}^{\ell}\frac{H(x)}{\sqrt{x}}\frac{H(-x)}{\sqrt{-x}}\,\mathrm{d}x = \frac{\pi}{2} \tag{112}$$

one may find

$$G(vt,v) = \frac{1}{4}\frac{\tilde{c}_{44}(s_a-\tilde{k}_e^2 s_l)+\tilde{c}_{44}'(s_a'-\tilde{k}_e'^2 s_l')}{\tilde{c}_{44}\tilde{c}_{44}'(s_a-\tilde{k}_e^2 s_l)(s_a'-\tilde{k}_e'^2 s_l')}\left(K_{IIIT}^{(\sigma)}(vt,v)\right)^2. \tag{113}$$

A convenient normalization is to the quasi-static elastic result

$$G(vt,0) := \frac{1}{4}\frac{\tilde{c}_{44}(1-\tilde{k}_e^2)+\tilde{c}_{44}'(1-\tilde{k}_e'^2)}{\tilde{c}_{44}\tilde{c}_{44}'(1-\tilde{k}_e^2)(1-\tilde{k}_e'^2)}(P(vt))^2. \tag{114}$$

The normalized energy release rate then reduces to

$$\frac{G(vt,v)}{G(vt,0)} = \frac{\tilde{c}_{44}(s_a - \tilde{k}_e^2 s_l) + \tilde{c}'_{44}(s'_a - \tilde{k}'^2_e s'_l)}{(s_a - \tilde{k}_e^2 s_l)(s'_a - \tilde{k}'^2_e s'_l)} \frac{(1-\tilde{k}_e^2)(1-\tilde{k}'^2_e)}{\tilde{c}_{44}(1-\tilde{k}_e^2) + \tilde{c}'_{44}(1-\tilde{k}'^2_e)} \frac{(1-v/c_{\mathrm{bg}})^2(1-v/c'_{\mathrm{bg}})^2}{(1-v/c)^2(1-v/c_a)} \times \frac{1}{(F_+(1/v))^2}. \tag{115}$$

As a check, let the materials of the upper and lower half spaces be the same, and Eq. (115) reduces to the result in [19]

$$\frac{G(vt,v)}{G(vt,0)} = \frac{(1-\tilde{k}_e^2)}{(s_a - \tilde{k}_e^2 s_l)} \frac{(1-v/c_{\mathrm{bg}})^2}{(1-v/c_a)} (\mathcal{T}_+(1/v))^2. \tag{116}$$

By letting $\tilde{k}_e, \tilde{k}'_e \to 0$, Eq. (115) reduces to the purely elastic result of dissimilar upper and lower space (e.g. [1]):

$$\frac{G(vt,v)}{G(vt,0)} = \frac{c_{44}\sqrt{1-v^2/c_0^2} + c'_{44}\sqrt{1-v^2/c'^2_0}}{(c_{44}+c'_{44})\sqrt{1-v^2/c_0^2}\sqrt{1-v^2/c'^2_0}} \frac{(1-v/c_0)}{(F^0_+(1/v))^2}, \tag{117}$$

where

$$F^0_+(\zeta) = \exp\left\{ -\frac{1}{\pi} \int_{1/(c_0-v)}^{1/(c'_0-v)} \arctan\left[ \frac{c_{44}\sqrt{1-v^2/c_0^2}\sqrt{(\zeta - 1/(c_0-v))(\zeta + 1/(c_0+v))}}{c'_{44}\sqrt{1-v^2/c'^2_0}\sqrt{(1/(c'_0-v)-\zeta)(\zeta+1/(c'_0+v))}} \right] \frac{\mathrm{d}\eta}{\eta+\zeta} \right\}, \tag{118}$$

where $c_0 = \sqrt{c_{44}/\rho}$ and $c'_0 = \sqrt{c'_{44}/\rho'}$ are the elastic shear wave velocities of the lower and upper half spaces, respectively. Furthermore, by letting $c_{44} = c'_{44}$ and $\rho = \rho'$, Eq. (118) reduces to the purely elastic result of identical upper and lower space (e.g. [9])

$$\frac{G(vt,v)}{G(vt,0)} = \frac{\sqrt{1-v/c_0}}{\sqrt{1+v/c'_0}}. \tag{119}$$

## 5. Discussions

Before examining the characteristics of the universal functions and the normalized energy release rate in detail, the physical context may be set by tabulating properties for several commonly used piezoelectric materials (Table 1). The corresponding electromechanical stiffened Young's modulus, shear wave speed, electromechanical coupling coefficient, and the Bleustein–Gulyaev wave speed are shown in Table 2. The materials chosen in the illustration cover a fairly large range of electro-mechanical coupling coefficients.

The first example is a classical problem in which a piezoelectric half space is welded to another one of the same material but in opposite polarity (i.e., $e_{15} = -e'_{15}$). It is similar to the interfaces in ferroelectric materials

Table 1
Material properties of several piezoelectric media

| Compound | $\rho$ (density) ($10^3$ kg/m$^3$) | $\epsilon^S_{11}$ ($10^{-9}$ F/m) | $c^E_{44}$ ($10^{10}$ N/m$^2$) | $e_{15}$ (C/m) |
|---|---|---|---|---|
| PZT-2 [2] | 7.6 | 4.4624 | 2.22 | 9.8 |
| PZT-5H [2] | 7.5 | 15.052 | 2.30 | 17.0 |
| ZnO [2] | 5.68 | 0.0757 | 4.25 | 0.48 |

Table 2
Electroacoustic constants of several piezoelectric materials

| Compound | $\bar{c}_{44} \equiv c^E_{44} + \frac{e^2_{15}}{\epsilon^S_{11}}$ ($10^{10}$ N/m$^2$) | $\tilde{k}_e \equiv \sqrt{\frac{e^2_{15}C_f}{\bar{c}_{44}\epsilon^S_{11}}}$ | $c_a \equiv \sqrt{\frac{\bar{c}_{44}}{\rho}}$ ($10^3$ m/s) | $c_{\mathrm{bg}} \equiv c_a\sqrt{\tilde{C}_f(1-\tilde{k}^4_e)}$ ($10^3$ m/s) |
|---|---|---|---|---|
| PZT-2 [2] | 4.3722 | 0.7016 | 2.3985 | 2.0878 |
| PZT-5H [2] | 4.2200 | 0.6745 | 2.3721 | 2.1123 |
| ZnO [2] | 4.5514 | 0.2586 | 2.8307 | 2.8244 |

with 180° domains. Under this condition, the existence of the Maerfeld–Tournois wave is always guaranteed. In fact, the Maerfeld–Tournois wave speed equals the Bleustein–Gulyaev wave speed, $c_{\mathrm{mt}} = c_{\mathrm{bg}} = c'_{\mathrm{bg}}$, and the universal functions, $g(v)$ and $g'(v)$, are identical. The universal functions for dynamic stress intensity factors are plotted against crack propagation speed, normalized by the slower Bleustein–Gulyaev wave speed $c'_{\mathrm{bg}}$ in Figs. 3a and b for each material listed in Table 2.

In Fig. 3c, the universal functions for a crack propagating along an interface between a PZT-5H and a PZT-2 half spaces in which the Maerfeld–Tournois wave exists are plotted; and Fig. 3d, the universal functions for a crack propagating along an interface between a PZT-5H and a ZnO half spaces in which the Maerfeld–Tournois wave does not exist are plotted. In each case, the universal function $f(v)$ decreases with increasing crack propagation velocity $v$ and reaches zero when $v$ reaches the slower Bleustein–Gulyaev velocity. The behaviors of the universal function $f(v)$ are similar to the universal function $k_{III}(v)$ of purely elastic solids, to which it reduces when $\tilde{k}_e, \tilde{k}'_e = 0$. However, the universal functions $g(v)$ and $g'(v)$ are more complicated and do not necessarily decrease to zero, when the crack speed reaches the slower Bleustein–Gulyaev wave speed.

In the second example, we consider an interface welded together by a piezoelectric upper half space and a elastic lower half space. The electro-mechanical coupling coefficient of the piezoelectric half space $\tilde{k}_e$ is allowed to increase from zero to unity while the material properties of the elastic half space are held constant.

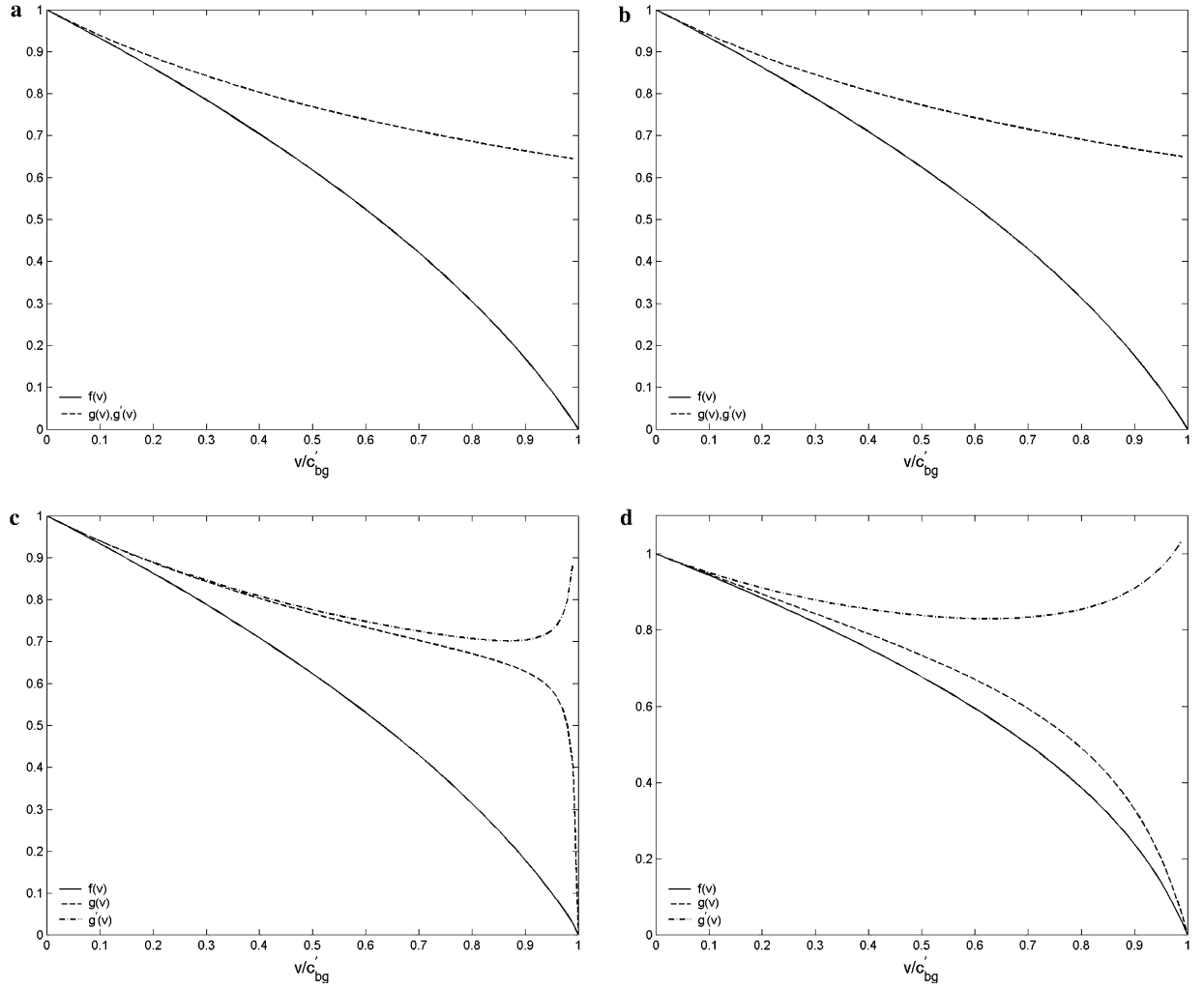


Fig. 3. Example 1: the universal functions, $f(v)$, $g(v)$, and $g'(v)$ for the following pairs of half spaces: (a) PZT-2 and PZT-2 with opposite polarity; (b) PZT-5H and PZT-5H with opposite polarity; (c) PZT-2 and PZT-5H; (d) PZT-5H and ZnO.

Figs. 4a–d display the universal functions and normalized energy release rate for a broad range of electro-mechanical coefficients ($\tilde{k}_e = 0.00, 0.30, 0.60, 0.90, 1.00$), with each plotted against the dimensionless velocity $v/c'_{\mathrm{bg}}$. Note that when $\tilde{k}_e = 0.00$, the solution degenerates to the case of two dissimilar purely elastic half spaces welded together as considered by Atkinson [1]. Furthermore, the universal function of the stress and the normalized energy release rate for the identical purely elastic case as considered by Eshelby [9] are plotted in thick solid lines for comparison. In the plot, as $\tilde{k}_e$ increases, the general behavior of all the universal functions and energy release rate remains nearly constant except when $\tilde{k}_e$ approaches unity, each universal function decreases dramatically. There are two competing wave effects here: with increasing $\tilde{k}_e$, the shear wave speed $c_a$ and the Bleustein–Gulyaev wave speed $c_{\mathrm{bg}}$ both increase, but the universal functions and energy release rate decreases with increasing $c_a$ while increases with larger $c_{\mathrm{bg}}$. However, since $c_{\mathrm{bg}}/c_a = \sqrt{\tilde{C}_f(1-\tilde{k}_e^4)}$, the term in the universal functions and energy release rate involving the shear wave speed dominates, so the overall effect is for the universal functions and the energy release rate to decrease. However, the effect is not significant at low values of $\tilde{k}_e$.

One may observe that as the crack velocity $v$ increases both $f(v)$, $g(v)$, and $G(vt, v)/G(vt, 0)$ decrease monotonically to zero while $g'(v)$ does not decrease to zero, but instead increases at low values of $\tilde{k}_e$ and high values of $v/c'_{\mathrm{bg}}$. The curious behavior of $g'(v)$ is attributed to the Bleustein–Gulyaev wave term $s'_a - \tilde{k}'^2_e s'_l$ in $g'(v)$. This term tends to zero as $v$ approaches the BG wave velocity $c'_{\mathrm{bg}}$ so that $g'(v)$ does not reach zero at large $v/c'_{\mathrm{bg}}$.

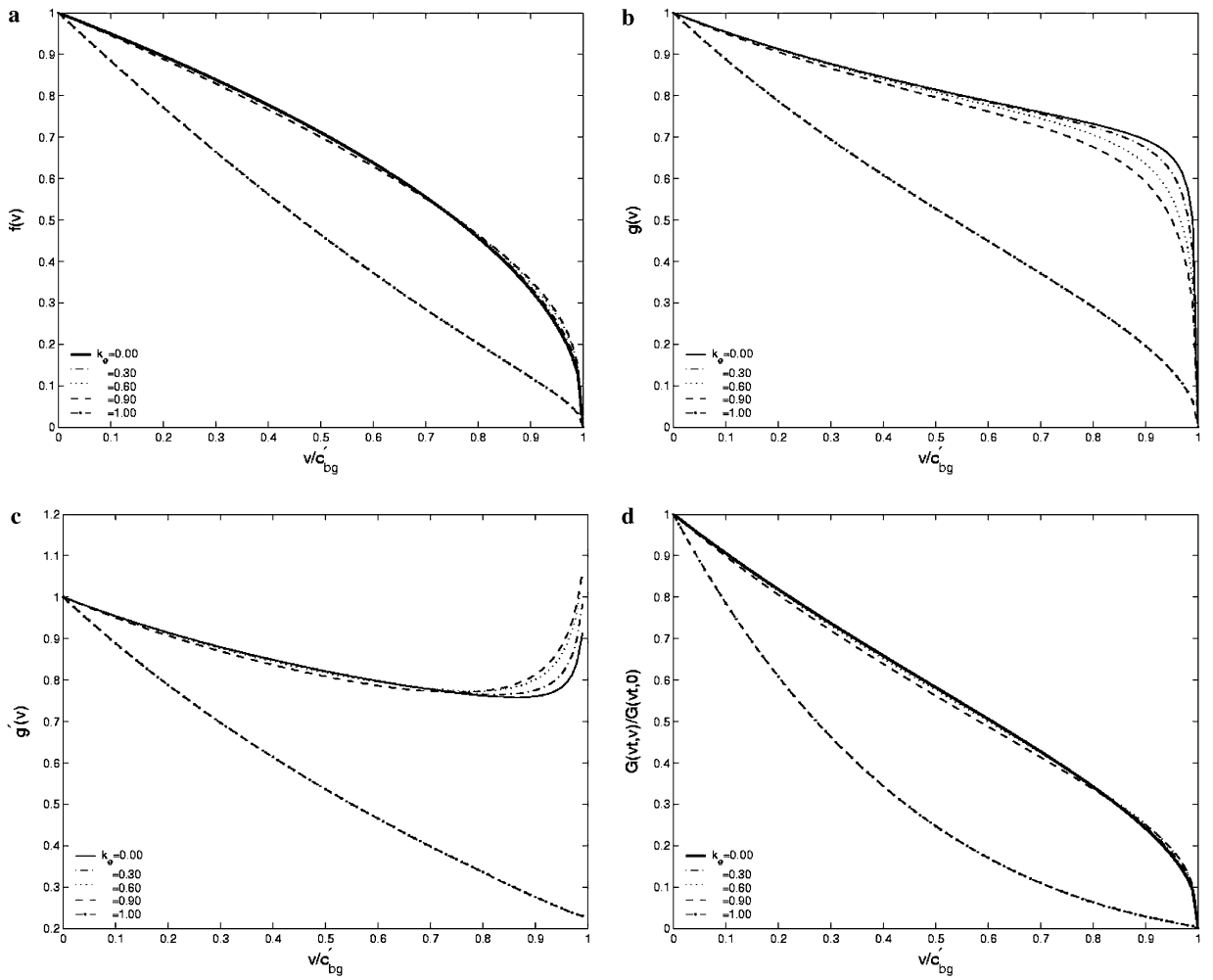


Fig. 4. Example 2: variations of universal functions (a) $f(v)$, (b) $g(v)$, (c) $g'(v)$, and (d) the normalized energy release rate $G(vt, v)/G(vt, 0)$ versus $v/c'_{\mathrm{bg}}$ for various electro-mechanical coupling coefficients $\tilde{k}_e$. The thick solid line in (a, d) is for the purely elastic identical media case.

Next, in the third example, we consider a piezoelectric half space with $\tilde{k}'_e = 0$ overlying another piezoelectric half space with $\tilde{k}_e = 0.70$, and the electro-mechanical coupling coefficient $\tilde{k}'_e$ of the upper half space is allowed to increase while the material properties of the lower piezoelectric half space are held constant. Figs. 5a–d display the universal functions and normalized energy release rate for a broad range of ratios of electro-mechanical coefficients $(\tilde{k}'_e/\tilde{k}_e = 0.00, 0.30, 0.60, 0.90, 1.00)$ plotted against the dimensionless velocity $v/c'_{bg}$. Note that when the ratio is unity, the model becomes two half space of identical piezoelectric materials as considered by [19]. As the ratio increases from zero to unity, the universal functions and the energy release rate decrease except at crack propagation velocities ($v$) near the Bleustein–Gulyaev wave velocity of the upper layer $c'_{bg}$. Note that when the ratio $\tilde{k}'_e/\tilde{k}_e = 0.00$, the Maerfeld–Tournois wave does not exist, but as the ratio $\tilde{k}'_e/\tilde{k}_e$ increases to 0.62, the MT wave begins to appear. Fig. 6 plots $c/c'_{bg}$ versus $\tilde{k}'_e/\tilde{k}_e$, where $c = c_{mt}$ if the Maerfeld–Tournois wave exists and $c = c'_a$ otherwise. Note from the figure that $c$ is always greater than or equal to $c'_{bg}$, and since $c'_{bg}$ increases with increasing $\tilde{k}'_e/\tilde{k}_e$, the effect of $c$ dominates and the overall effect is for the universal functions and energy release rate to decrease. Examining their behavior more closely for all electro-mechanical ratios, we find that $f(v)$, $g(v)$, and $G(vt, v)/G(vt, 0)$ decrease monotonically to zero with increasing $v/c'_{bg}$ except at $\tilde{k}'_e/\tilde{k}_e = 0.00$ where $g(v) = g'(v)$ does not decrease to zero. Also, $g'(v)$ does not decrease to zero for increasing $v/c'_{bg}$ but instead increases at low electro-mechanical ratios and high crack propagation velocities. As in the previous case, the curious behavior of $g'(v)$ is attributed to the Bleustein–Gulyaev wave

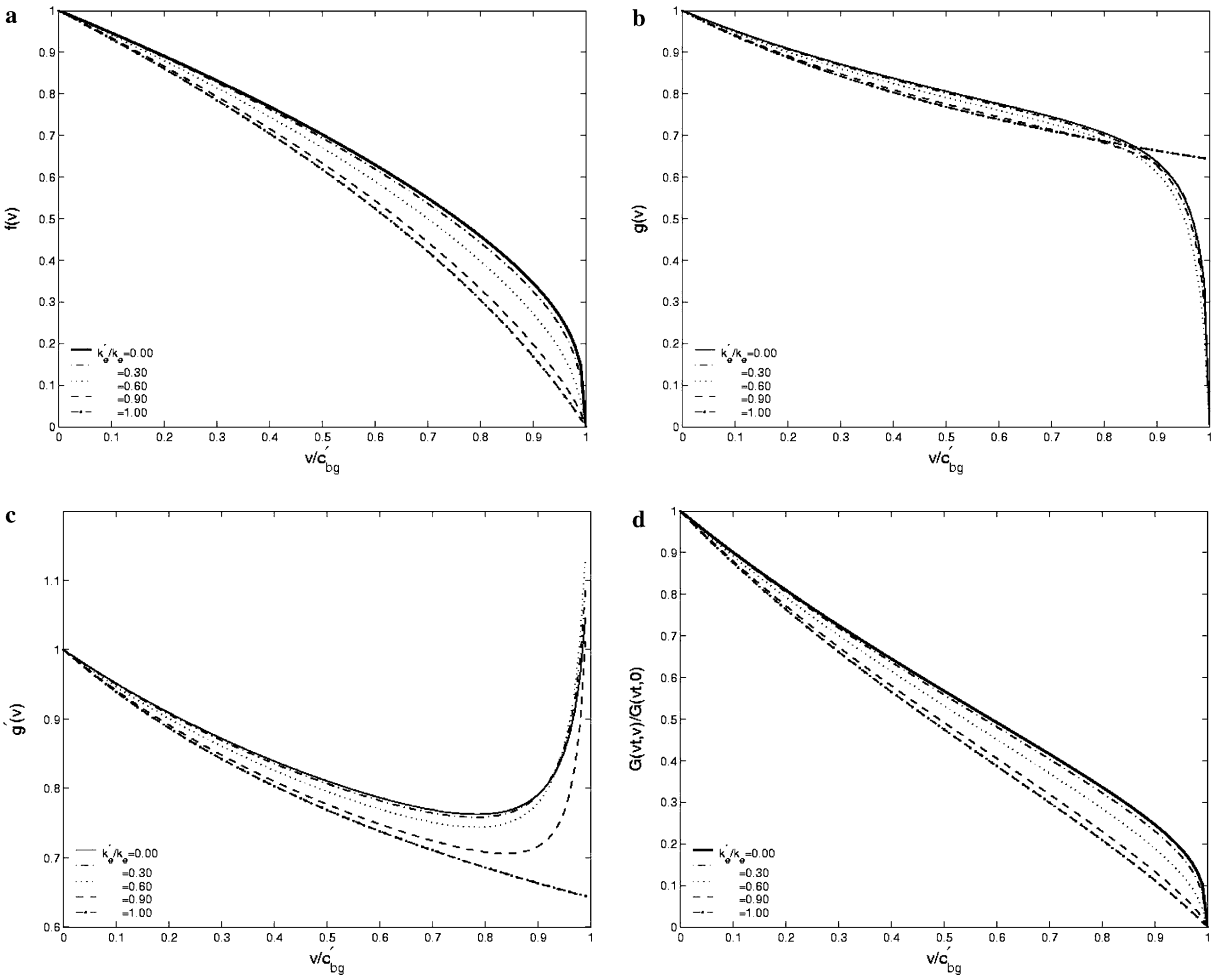


Fig. 5. Example 3: variations of universal functions (a) $f(v)$, (b) $g(v)$, (c) $g'(v)$, and (d) the normalized energy release rate $G(vt, v)/G(vt, 0)$ versus $v/c'_{bg}$ for various electro-mechanical coupling ratios $\tilde{k}'_e/\tilde{k}_e$.

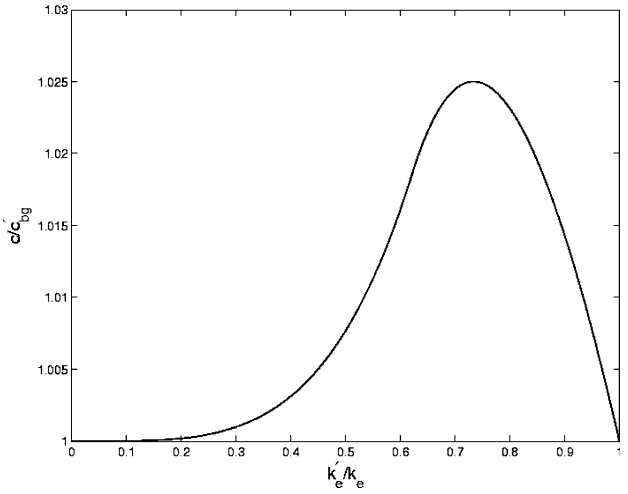


Fig. 6. Variations of velocities $(c/c'_{bg})$ versus electro-mechanical coupling ratio $(\tilde{k}'_e/\tilde{k}_e)$.

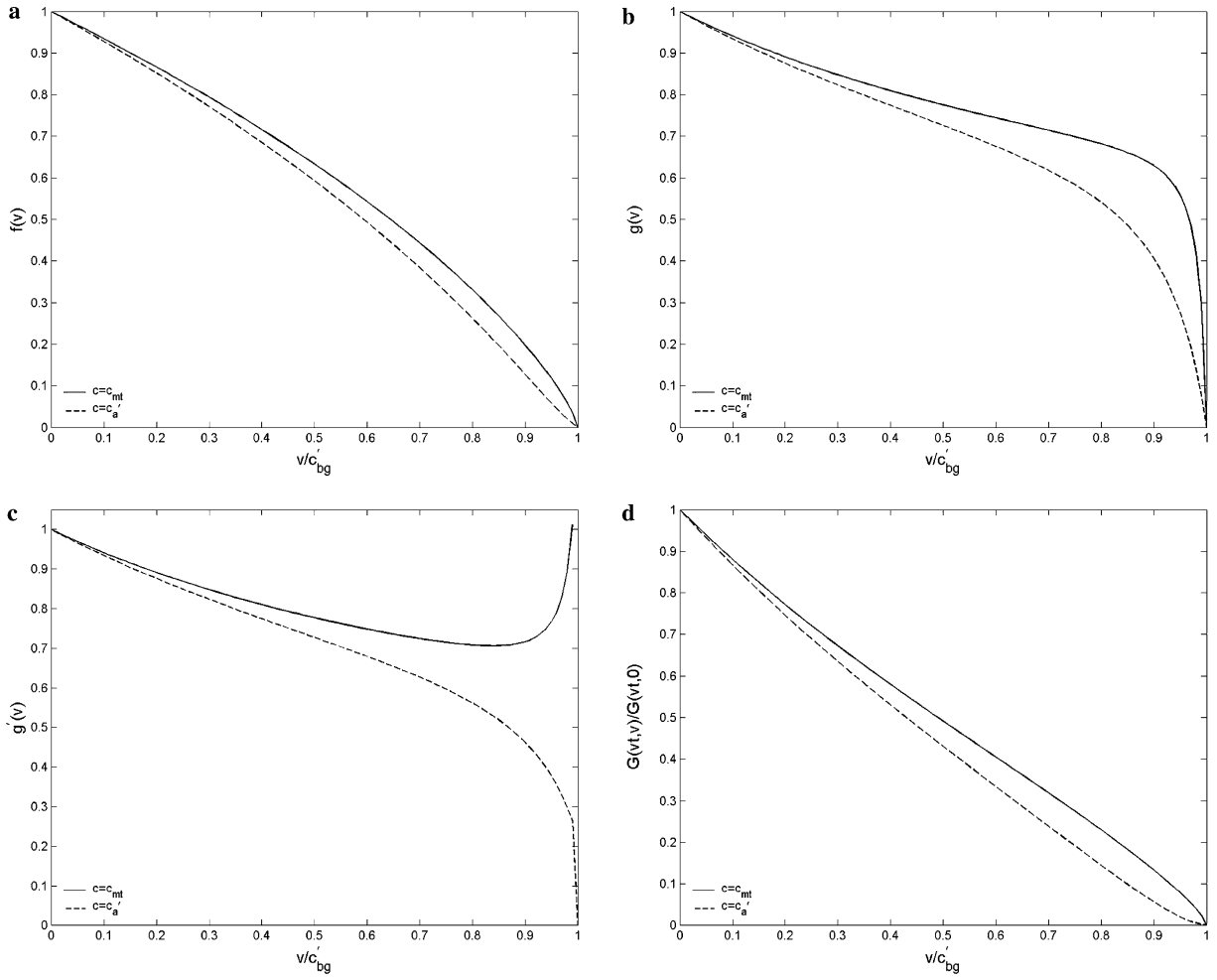


Fig. 7. Example 4: variations of universal functions (a) $f(v)$, (b) $g(v)$, (c) $g'(v)$, and (d) the normalized energy release rate $G(vt,v)/G(vt,0)$ versus $v/c'_{bg}$ when the Maerfeld–Tournois wave exists (solid line) and when it does not exist (dashed line).

term $s'_a - \tilde{k}'^2_e s'_l$ in $g'(v)$ because it tends to zero as $v$ approaches the BG wave velocity so that $g'(v)$ does not reach zero at large $v/c'_{bg}$ (see Fig. 5d).

In the last example, it is not clear exactly how the existent Maerfeld–Tournois wave affects the universal functions and the normalized free-energy release rate, because change in the electro-mechanical coupling ratio causes the BG wave speed to change as well. Here, we compared these quantities with a classical example: in the first case, the upper and lower half spaces have identical properties, while in the second case, everything is the same as the first case except that the polarity is different (i.e., $e'_{15} = -e_{15}$). The Maerfeld–Tournois wave does not exist in the first case while it is guaranteed to exist in the second case. Notice that the light wave velocity $v_\ell$, the shear wave velocity $v_a$, the BG wave velocities $v_{bg}$, and the electro-mechanical coupling coefficient $\tilde{k}_e$ are identical for the two cases. To compare the universal functions and the normalized energy release rate, the ratios for the first and the second case are derived from Eqs. (107)–(109) and (115):

$$Ra(f(v)) = Ra(g(v)) = Ra(g'(v)) = \frac{(1 - v/c_{mt})}{(1 - v/c_a)}, \tag{120}$$

$$Ra\left(\frac{G(vt, v)}{G(vt, 0)}\right) = \frac{(1 - v/c_{mt})^2}{(1 - v/c_a)^2} \leqslant 1.0, \tag{121}$$

where $Ra(\cdot)$ is the ratio of the quantity of interest of the first case to that of the second case. Since the Maerfeld–Tournois wave velocity is always less than the shear wave velocity, these ratios are always less than one. In other words, the universal functions and the normalized energy release rate are always higher at the same crack propagating velocity when the Maerfeld–Tournois wave exists, even when the electro-mechanical coupling coefficient is identical in both cases as shown in Fig. 7. This result can be justified in qualitative terms: *An interfacial surface wave can supply more energy to a crack to create new surface, or, the existence of the MT interfacial surface wave traps additional energy on crack surfaces, which may propel the crack propagation.*

## 6. Conclusions

In this work, we have studied dynamic fracture of an interfacial crack in dissimilar piezoelectric media. First, we have observed that in all universal functions for dynamic intensity factors the effects of the Bleustein–Gulyaev waves of the upper and lower half space are competing with those of the faster shear wave and the Maerfeld–Tournois wave (or the slower shear wave if the MT wave does not exist). The competing effects in turn depend on the electro-mechanical coefficients $(\tilde{k}_e, \tilde{k}'_e)$ where the higher the electro-mechanical coefficient, the lower the nondimensional stress intensity factor and the dynamic free-energy release rate. Second, the existence of the Maerfeld–Tournois wave will increase the dynamic intensity factors and the dynamic free-energy release rate. Nevertheless, the lowest stress intensity and free-energy release rate are always controlled by the slower Bleustein–Gulyaev wave; that is, the limiting crack propagating velocity $v_{limit}$ equals to the slower BG wave $c'_{bg}$. In conclusion, it may be possible that for two piezoelectric interfaces with the same electro-mechanical coupling coefficient, the interface that allows the existence of the Maerfeld–Tournois wave will have relative weak interface strength, and the interface that excludes the possibility of the Maerfeld–Tournois wave will have higher interface fracture toughness.

## Acknowledgements

The authors thank the two anonymous referees for their comments, suggestions, and encouragement. This research is partially supported by Jane Lewis Fellowship from University of California, Berkeley (A.C.T.), a grant from NSF (Grant No. CMS-0239130) (S.L.), and another grant from NSF (Grant No. CMS-9908218) (S.D.G.), which are gratefully acknowledged.

## References

[1] C. Atkinson, Dynamic crack problems in dissimilar media, in: G.C. Sih (Ed.), Mechanics of Fracture 4: Elastodynamic Crack Problems, Noordhoff, London, 1977, pp. 213–228, Chapter 4.

[2] B.A. Auld, Acoustic Fields and Waves in Solids, Wiley, New York, 1973 (Two volumes).
[3] J.L. Bleustein, A new surface wave in piezoelectric materials, Appl. Phys. Lett. 13 (1968) 412–413.
[4] L.M. Brock, Interface crack extension at any constant speed in orthotropic or transversely isotropic bimaterials – i. general exact solutions, Int. J. Solids Struct. 39 (2002) 1165–1182.
[5] L. Cagniard, Reflexion et Refraction des Ondes Seismiques Progressives, Gauthier-Villars, Paris, 1939. English translation Reflection and Refraction of Progressive Seismic Waves by E.A. Flinn and C.H. Dix, 1962, McGraw-Hill.
[6] C. Dascalu, G.A. Maugin, Energy-release rates and path-independent integrals in electroelastic crack propagation, Int. J. Eng. Sci. 32 (1994) 755–765.
[7] C. Dascalu, G.A. Maugin, On the dynamic fracture of piezoelectric materials, Q. J. Mech. Appl. Math. 48 (1995) 237–255.
[8] A.T. de Hoop, A modification of cagniard's method for solving seismic pulse problems, Appl. Sci. Res. B8 (1960) 349–360.
[9] J.D. Eshelby, The starting of a crack, in: A.S. Argon (Ed.), Physics of Strength and Plasticity, MIT Press, Cambridge, MA, 1969, pp. 213–248.
[10] L.B. Freund, Crack propagation in an elastic solid subjected to general loading. I: constant rate of extension, J. Mech. Phy. Solids 20 (1972) 120–140.
[11] L.B. Freund, Dynamic Fracture Mechanics, Cambridge University Press, Cambridge, 1990.
[12] H. Gao, T.-Y. Zhang, P. Tong, Local and global energy release rates for an electrically yielded crack in a piezoelectric ceramic, J. Mech. Phys. Solids 45 (1997) 491–510.
[13] Y.V. Gulyaev, Electrocoustic surface waves in solids, Sov. Phys. JETP 9 (1969) 37–38.
[14] Y.S. Ing, M.J. Wang, Explicit transient solutions for a mode iii crack subjected to dynamic concentrated loading in a piezoelectric material, Int. J. Solids Struct. 41 (2004) 3849–3864.
[15] S. Li, The electromagneto-acoustic surface wave in a piezoelectric medium: the Bleustein–Gulyaev mode, J. Appl. Phys. 80 (1996) 5264–5269.
[16] S. Li, Transient wave propagation in a transversely isotropic piezoelectric half space, Z. Angew. Math. Phys. 51 (2000) 236–266.
[17] S. Li, On diffraction in a piezoelectric medium by half-plane: the sommerfeld problem, Z. Angew. Math. Phys. 52 (2001) 101–134.
[18] S. Li, On saturation-strip model of a permeable crack in a piezoelectric ceramic, Acta Mech. 165 (2003) 47–71.
[19] S. Li, P.A. Mataga, Dynamic crack propagation in piezoelectric materials, part I: electrode solution, J. Mech. Phys. Solids 44 (1996) 1799–1830.
[20] S. Li, P.A. Mataga, Dynamic crack propagation in piezoelectric materials, part II: vacuum solution, J. Mech. Phys. Solids 44 (1996) 1831–1866.
[21] C. Maerfeld, P. Tournois, Pure shear elastic surface wave guided by the interface of two semi-infinite media, Appl. Phys. Lett. 19 (1971) 117.
[22] F. Narita, Y. Shindo, Dynamic anti-plane shear of a cracked piezoelectric ceramic, Theor. Appl. Fract. Mech. 29 (1998) 169–180.
[23] B. Noble, Methods Based on the Wiener–Hopf Technique, Pergamon Press, New York, 1958.
[24] Y.E. Pak, Crack extension force in a piezoelectric material, J. Appl. Mech. 57 (1990) 647–653.
[25] S. Park, C.T. Sun, Effect of electric field on fracture of piezoelectric ceramics, Int. J. Fracture 70 (1995) 203–216.
[26] S. Park, C.T. Sun, Fracture criteria for piezoelectric ceramics, J. Am. Ceram. Soc. 78 (1995) 1475–1480.
[27] C.Q. Ru, Electrode-ceramic interfacial cracks in piezoelectric multilayer materials, J. Appl. Mech. 67 (2000) 255–261.
[28] C.Q. Ru, Exact solution for finite electrode layers embedded at the interface of two piezoelectric half-planes, J. Mech. Phys. Solids 48 (2000) 693–708.
[29] C.Q. Ru, X. Mao, Conducting cracks in a piezoelectric ceramic of limited electrical polarization, J. Mech. Phys. Solids 47 (1999) 2125–2146.
[30] C.Q. Ru, X. Mao, M. Epstein, Electric-field induced interfacial cracking in multilayer electrostrictive actuators, J. Mech. Phys. Solids 46 (1998) 1301–1318.
[31] Y. Shindo, E. Ozawa, Dynamic analysis of a cracked piezoelectric material, in: R.K.T. Hsieh (Ed.), Mechanical Modelling of New Electromagnetic Materials, Elsevier, Amsterdam, 1990, pp. 297–304.
[32] A.C. To, S. Li, S.C. Glaser, On scattering in dissimilar piezoelectric materials, by a semi-infinite interfacial crack, Q. J. Mech. Appl. Math. 58 (2005) 309–331.
[33] T.Y. Zhang, M. Zhao, P. Tong, Fracture of piezoelectric ceramics, in: E. ven der Giessen, T.Y. Wu (Eds.), Advances in Applied Mechanics, vol. 38, Academic Press, New York, 2001, pp. 147–289.